Acta Materialia 151 (2018) 424–431

Contents lists available at ScienceDirect

Acta Materialia

journal homepage: www.elsevier.com/locate/actamat

Full length article

Adiabatic shear localization in the CrMnFeCoNi high-entropy alloy

Zezhou Li [a], Shiteng Zhao [a], Senhat M. Alotaibi [a], Yong Liu [b], Bingfeng Wang [b], Marc A. Meyers [a, *]

[a] University of California, San Diego, La Jolla, CA, USA
[b] Central South University, Changsha, Hunan, PR China

ARTICLE INFO

Article history:
Received 17 November 2017
Received in revised form
20 March 2018
Accepted 21 March 2018
Available online 2 April 2018

Keywords:
The CrMnFeCoNi HEA
Mechanical response
Adiabatic shear band

ABSTRACT

The mechanical behavior of the single phase (fcc) CrMnFeCoNi high-entropy alloy (HEA) is examined in the dynamic regime. A series of experiments by dynamic-loading hat-shaped specimens using stopper rings to control the displacement are performed, and the alloy resists adiabatic shear-band formation up to a very large imposed shear strain of ~7. It is proposed that the combination of the excellent strain-hardening ability and moderate thermal-softening effect retard shear localization. Recrystallized ultrafine-grained grains (diameters of 100–300 nm) with twins are revealed inside the shear band. Their formation is explained by the rotational dynamic recrystallization mechanism. The stability of the structure at high strain rates strongly suggests a high ballistic resistance for this class of alloys.

1. Introduction

The dynamic properties of materials are of great importance in applications involving ballistic impact and penetration [1]. Adiabatic shear localization is recognized as an important failure mechanism of materials and is produced by the temperature rise in a narrow region, especially formed under high strain-rate deformation, when the deformation time is lower than the heat diffusion time. The formation of nanostructured and ultrafine grains inside the shear band by dynamic recrystallization has been widely studied [2,3]. The mechanism that leads to this microstructure is similar to the one operating in severe plastic deformation, a widely used method to produce nanostructured metals [4].

The high-entropy alloy (HEA) design strategy is based on five or more elements mixed in equiatomic or near-equiatomic concentrations, such that the high configurational entropy ΔS_{Conf} promotes single-phase solid solution formation [5]. Cantor et al. [6] developed the CrMnFeCoNi HEA with the single face-centered-cubic (fcc) phase and therefore this alloy is also known as the "Cantor alloy". Recently, Gludovatz et al. [7] found that this CrMnFeCoNi HEA achieved remarkable damage-tolerance with a tensile strength around 1 GPa and fracture toughness exceeding 200 MPa $m^{1/2}$. Furthermore, its mechanical properties improved at cryogenic temperatures due to the transition of deformation mechanism from planar dislocation slip to mechanical nano-twinning. In-situ TEM experiments by straining a thin foil containing cracks revealed a synergy of multiple deformation mechanisms of this alloy, rarely achieved in other metallic systems. These mechanisms include the easy motion of the Shockley partials, their interactions to form stacking-fault parallelepipeds, and arrest at planar slip bands of perfect dislocations. The multiple deformation modes of the Cantor alloy lead to high strength, high work-hardening rate and good ductility [8]. The quasi-static mechanical behavior of the HEAs has been widely studied, as reviewed by Zhang et al. [9]. Other physical and mechanical properties, such as a combination of high strength and good ductility for the $Cr_{10}Mn_{30}Fe_{50}Co_{10}$ high-entropy steel [10], phase evolution of the $Al_{1.3}CoCrCuFeNi$ HEA at elevated temperatures (from 800 to 1400 °C) [11], and excellent fatigue behavior of $Al_{0.5}CoCrCuFeNi$ two-phase high-entropy alloy [12,13], have also been established. However, the dynamic properties of HEAs are insufficiently unexplored. Only one study stands out: that of $Al_{0.3}CoCrFeNi$ HEA which shows a significant resistance to shear banding. Therefore, the aim of this investigation is to study the dynamic properties of the Cantor alloy, especially its resistance to shear localization.

2. Experimental procedures

The as-received CrMnFeCoNi HEA was prepared by the spark plasma sintering (SPS) method [14]. The XRD characterization

* Corresponding author.
E-mail address: mameyers@eng.ucsd.edu (M.A. Meyers).

https://doi.org/10.1016/j.actamat.2018.03.040
1359-6454/

experiment on the as-received material was made by Cu Kα radiation from 20° to 90° (2θ) with a scanning speed of 2.8°/min and a step size of 0.014°. The sample was prepared by the standard mechanical grinding and polishing method. The chemical composition analysis was conducted by energy-dispersive x-ray (EDX) spectroscopy in a Phillips XL30 scanning electron microscopy (SEM). Quasi-static experiments were carried out in an Instron universal testing machine. Dynamic compression tests were performed using a split-Hopkinson pressure bar (SHPB). The dynamic mechanical properties and shear deformation were measured using cylindrical and hat-shaped specimens. The cylinders had a length of 4 mm and a diameter of 4 mm. Hat-shaped specimens with stopper rings were used to generate high shear strain in the "forced" localized region. The samples were polished and then etched by a dilute aqua regia solution before microstructural examination. The shear band was examined in a Phillips XL30 SEM. A focused ion beam (FIB) instrument was used to accurately prepare TEM samples in the shear band region. The FIB samples were then characterized by TEM using a FEI Tecnai G^2 Polara transmission electron microscope operating at 200 kV.

3. Results and discussion

Fig. 1 shows the homogeneous distribution of 5 elements of CrMnFeCoNi HEA and corresponding chemical compositions with each element around 20% (in atomic percentage). Fig. 2(a) shows the initial microstructure of this alloy, which contains coarse-grained grains. Fig. 2(b) shows grain size distribution from Fig. 2(a) measured by the line intercept method [15]: the average grain size of as-received HEA is 8 μm. The presence of annealing twins [16] is inversely related to the stacking fault energy, which has been reported to be ~20 mJ/m^2 for the Cantor alloy by Zaddach et al. [17]. The X-ray diffraction (XRD) scan in Fig. 2(c) shows that this alloy contains a single fcc structure. While three components (Cr, Mn and Fe) have the body-centered cubic crystalline structure, one (Co) presents the hexagonal close-packed structure, and only Ni has the face-centered cubic structure. The measured *d*-spacings from the X-ray diffraction results are almost the same as the reported values [18]; the lattice constant of CrMnFeCoNi HEA is 3.596 Å obtained by linear interpolation. For comparison, the results are summarized in Table 1. EDX spectroscopy and XRD results indicate the equiatomic elemental distribution and single-phase character of the as-received high-entropy alloy.

In order to promote shear localization, a special geometry was used in dynamic testing. This hat-shaped configuration, originally developed by Meyer and Manwaring [19], is well known and has been used for over thirty years (e. g., [20–24]). Fig. 3(a) shows the dimensions of the hat-shaped specimen, which was deformed at room temperature to induce a forced shear band using a split-Hopkinson pressure bar. A series of dynamic-loading experiments on hat-shaped specimens using stopper rings to control the displacement (0.7, 1.14, 1.57 and 2 mm) were performed. However, among these specimens, a clear shear band was only found at a very large imposed shear strain of ~7. The corresponding shear stress vs. shear strain curve is illustrated in Fig. 3(b). The work imposed upon the material during deformation can be used to calculate an (adiabatic) temperature rise inside the shear band [1]:

$$dT = \frac{0.9}{\rho C_p}\tau d\gamma \tag{1}$$

where $\rho = 7.9\ kg/m^3$ is the density and C_p is the specific heat capacity. The specific heat capacity C_p of the Cantor alloy is approximated to be 450 J/(kg K) by using a weight averaging method $C_p = \omega_i \sum_{i=1}^{5} C_{pi}$ (ω_i is the weight percent and C_{pi} is the specific heat capacity for each element of the alloy) [25]. Fig. 3(b) shows that the temperature can rise to about 700 K inside the shear band, which approaches the recrystallization temperature for the Cantor alloy, $0.4T_m$, its melting temperature being around 1600 K [26].

Fig. 3(c) shows the microstructure inside and outside the shear band. The particles were separated at the grain boundaries under severe plastic deformation as shown by the inserts of Fig. 3(c). Fig. 3(c) shows that the alloy fractures along grain boundaries under dynamic impact. The microvoids resulting from residual porosity in the SPS process can easily nucleate and propagate cracks along grain boundaries. Similar fracture behavior has been

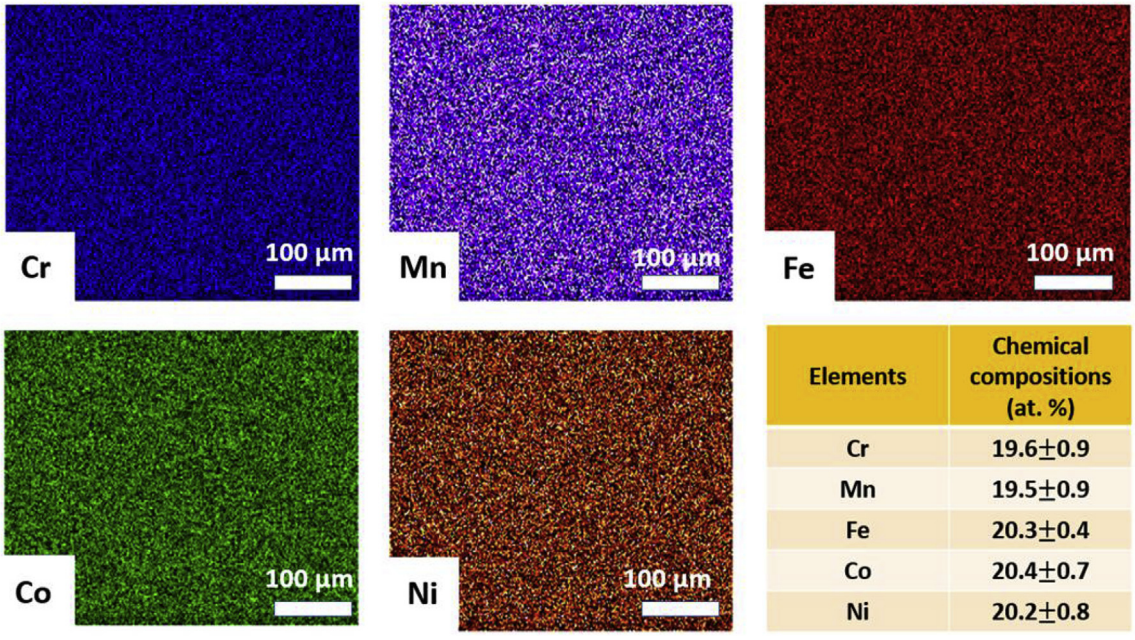

Elements	Chemical compositions (at. %)
Cr	19.6±0.9
Mn	19.5±0.9
Fe	20.3±0.4
Co	20.4±0.7
Ni	20.2±0.8

Fig. 1. Elemental mapping of the CrMnFeCoNi HEA and corresponding chemical compositions by scanning electron microscopy (SEM)-Energy-dispersive X-ray spectrometry (EDX).

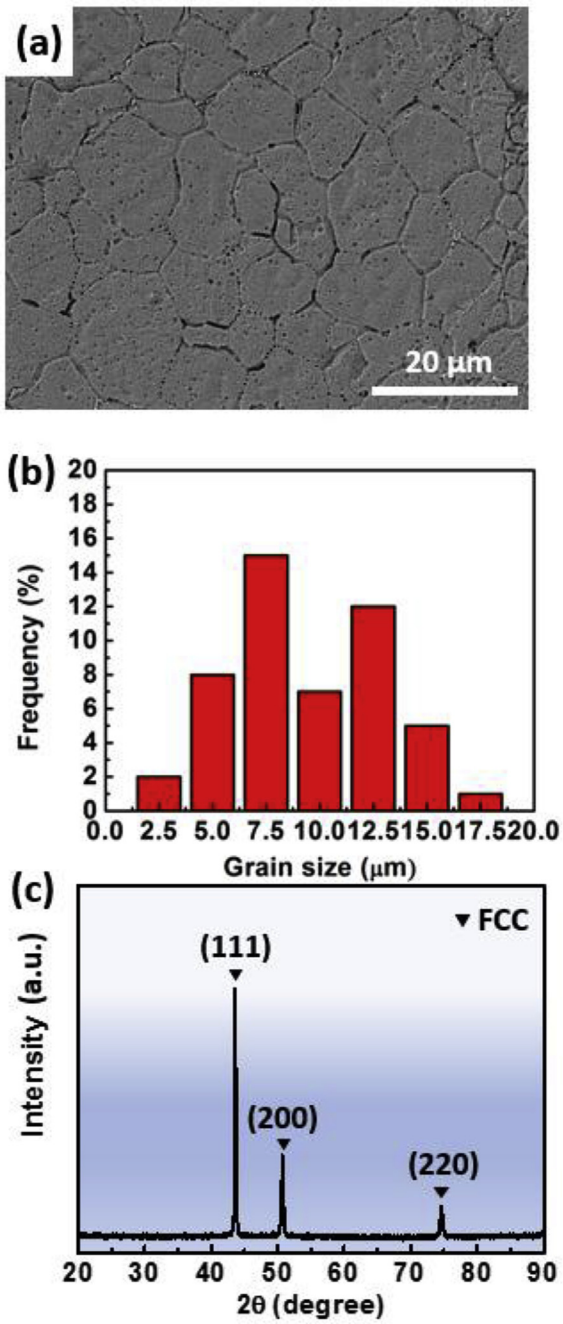

Fig. 2. (a) Scanning electron microscopy image of initial microstructure of the CrMnFeCoNi HEA; (b) grain size distribution in Fig. (a); (c) X-ray diffraction pattern of the CrMnFeCoNi HEA.

observed earlier in this alloy under high strain-rate impact [14]. However, these peripheral cracks did not affect the shear-localization zone and do not interfere with the results of this work. A zoom-in image in Fig. 3(d) shows that the shear band width is about 10 μm. Focused ion beam (FIB) method was used to lift out the transmission electron microscope (TEM) site-specific specimens inside the shear band. The formation mechanism of the shear bands in metals has been widely studied [3]. It is accepted that shear bands are formed when the thermal softening effect overdrives the strain and strain-rate hardening effects. This is expressed analytically as [27]:

$$\frac{d\tau}{d\gamma} = \left(\frac{\partial\tau}{\partial\gamma}\right)_{\dot{\gamma},T} + \left(\frac{\partial\tau}{\partial\dot{\gamma}}\right)_{\gamma,T}\frac{d\dot{\gamma}}{d\gamma} + \left(\frac{\partial\tau}{\partial T}\right)_{\dot{\gamma},\gamma}\frac{dT}{d\gamma} \leq 0 \tag{2}$$

The first term represents work hardening; the second, strain-rate hardening, and the third, thermal softening. Therefore, materials with higher hardenability as well as lower thermal softening ability usually possess a high resistance to shear localization.

The mechanical response of the Cantor alloy was established at strain rates varying from 10^{-4} s^{-1} to 1600 s^{-1} to examine its strain-hardening effect. The compressive true stress vs. true strain curves are shown in Fig. 4(a). Under both quasi-static and dynamic compression, the strength of this alloy increases gradually with increasing strain. The fluctuations in the stress-strain curve at high strain-rate were due to the nature of elastic wave propagation in cylinder bars: the "dispersion" effect [1]. In the Hopkinson bar test, the bar has radial inertia and a wave interacts with the external surfaces of cylinder bars (free surfaces). Radial inertia is caused by the kinetic energy of material flowing radially outward as the bar is compressed. This causes the decrease in the slope of the rise of the wave and was reflected in the stress-strain curve. The strain-hardening rate (measured by slope of the curve at a true strain of 0.2) is ~1100 MPa, similar to that of the $Al_{0.3}$CoCrFeNi HEA [28]. This strain hardening is maintained at 1600 s^{-1}, which is evidence that no localization is taking place. This same resistance to shear localization has been reported for the $Al_{0.3}$CoCrFeNi HEA [28]; it was attributed to good strain-hardening ability, caused by solid-solution hardening, forest-dislocation hardening, as well as mechanical twinning. Otto et al. [29] also reported that the strain-hardening rate in tension of the CrMnFeCoNi HEA can be higher than 1000 MPa at low temperature (77 K). This excellent strain-hardening ability is mainly due to multiple nanotwinning deformation. Deformation twinning, by continually introducing new interfaces and decreasing the mean free path of dislocations during deformation, can generate a high degree of work-hardening. Thus, to activate shear localization in CrMnFeCoNi HEA, a very large shear strain and shear stress need to be imposed on specimens to increase the thermal-softening effect.

Starting from Eq. (2), Staker [30] proposed an expression for critical shear strain for shear localization (neglecting the effect of strain-rate hardening):

$$\gamma_c = \frac{\rho C_p n}{-\frac{\partial\tau}{\partial T}} \tag{3}$$

where ρ is the density, C_p is the specific heat capacity, n is the strain-hardening power index in the Ludwik-Hollomon constitutive equation ($\tau = \tau_0 + K\gamma^n$, where τ_0 is the yield stress and K is a constant), and $\frac{\partial\tau}{\partial T}$ is the thermal-softening parameter. Eq. (3) expresses the competition between strain hardening and thermal softening prior to shear localization. The normal stress and normal strain can be converted into shear stress and shear strain by: $\tau = \sigma/2$ and $\gamma = \sqrt{2\exp(2\varepsilon) - 1} - 1$ [31]. Fig. 4(b) shows the value $\rho C_p n$ for pure Ti [32], Ti-6Al-4V alloy [33], AISI 1006 steel [34], copper [34], brass [34], and the Cantor alloy. As stated before, from Eqn. (3), the value of $\rho C_p n$ can be regarded as the hardening component,

Table 1
d-spacings (in Å) of the different (hkl) planes of the fcc CrMnFeCoNi HEA measured by different testing methods.

Methods	*d* (111)	*d* (200)	*d* (220)
XRD (X-ray diffraction)	2.076	1.801	1.273
TEM (selected area diffraction)	2.058	1.780	1.223
XRD (X-ray diffraction) [18]	2.076	1.798	1.271

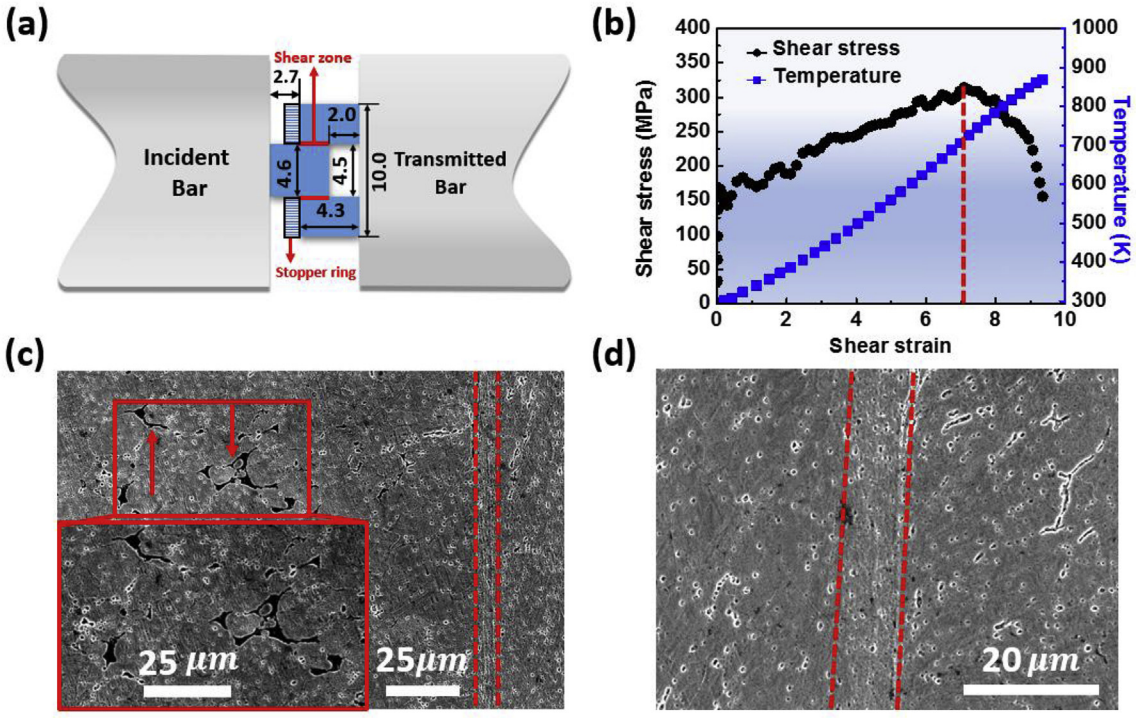

Fig. 3. (a) Schematic drawing of dynamic loading of the hat-shaped specimen with the stopper ring (in mm) by the split-Hopkinson pressure bar; (b) shear stress, shear strain and temperature evolution of the shear band; (c) scanning electron microscope (SEM) image showing separation of particles near the shear band; (d) SEM image of the shear band.

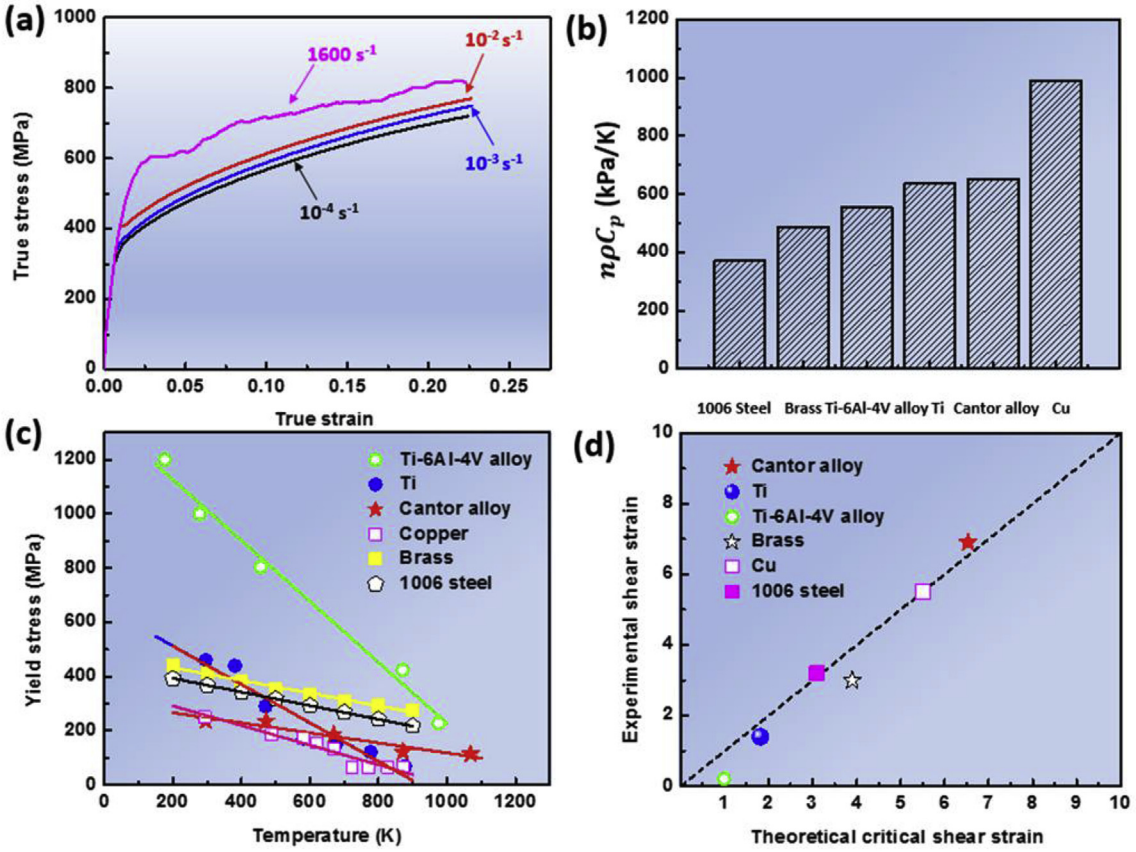

Fig. 4. (a) Mechanical response of the Cantor alloy under different strain-rates; (b) the value of $\rho C_p n$ for pure Ti [32], Ti-6Al-4V alloy [33], 1006-Steel [34], Copper [34], Brass [34] and the Cantor alloy; (c) thermal-softening effect of different materials [22,32,33,35,36]; (d) experimental and predicted critical shear strain for shear localization [34,36].

while the $\frac{\partial \tau}{\partial l}$ is the thermal-softening parameter. Fig. 4(b) shows that Cu has the highest $\rho C_p n$ value. The value of $\rho C_p n$ for CrMnFeCoNi HEA is about 70% of that of Cu and it is slightly higher than that of Ti. Understandingly, it is very difficult to induce shear localization in copper. In addition, Fig. 4(c) shows that the Cantor alloy has the smallest thermal softening effect [35] in the temperature range from 200 K to 1000 K, in comparison with titanium [32], Ti-6Al-4V alloy [33], AISI 1006 steel [36], copper [22], and brass [36]. Otto et al. [29] reported that the CrMnFeCoNi HEA did not lose its yield strength until 873 K with a sudden drop of strength. The melting temperature of the CrMnFeCoNi HEA is 1614 K as reported by Laurent-Brocq et al. [37]. This is as high as that (about 1600 K) [38] of Inconel 718 superalloy. Miracle et al. [39] found superior high temperature behavior of NbMoTaW and VNbMoTaW HEAs compared with conventional alloys since they did not lose their strength till 1000 K. Tsai et al. [40] found that interaction energy (which is the excess free energy that arises when two unlike atoms bond with each other) of Ni element in $CrMn_{0.5}FeCoNi$ HEA is higher than that in Cr-Fe-Ni alloy. This leads to a sluggish diffusion effect and also indicates that it needs higher thermal energy to break up metallic bonds in HEAs than in conventional alloys. Thus, the small thermal softening effect of the CrMnFeCoNi HEA can promote the resistance to shear localization. Fig. 4(d) shows the predicted critical shear strain for shear localization in these metals using Eqn. (3). Fig. 3(b) shows that the adiabatic shear band is formed only at a very large shear strain ~7. It should be noted that the imposed shear deformation region has a width of over 50 μm whereas the adiabatic shear band has a width of ~10 μm. Therefore, the combination of the excellent strain-hardening ability and moderate thermal-softening of the Cantor alloy postpones shear localization to higher levels of shear deformation.

Fig. 5(a) shows the microstructure inside the adiabatic shear band. It indicates that the Cantor alloy goes through significant grain refinement. The grain size inside the shear band ranges from 100 to 300 nm. These equiaxed ultrafine-grained grains are formed by significant dynamic recrystallization. The corresponding dark-field image in Fig. 5(b) confirms the nanostructured recrystallized grains inside the shear band. The diffraction pattern in Fig. 5(c) shows that it is a polycrystalline material without strong texture, indicating a fully recrystallized microstructure inside the shear band. The *d*-spacings of the CrMnFeCoNi HEA measured from SAD pattern (as shown in Table 1) show minor differences with those measured from XRD pattern, which may be attributed to the more severe deformation inside the shear band than the bulk material. The grain size was measured using the mean linear intercept method [15]. Fig. 5(d) shows that grains inside the shear band break into both ultrafine-grained and nanocrystalline regimes. Lee et al. [41] reported that CrMnFeCoNi HEA retains a single-phase fcc recrystallized structure under high-pressure (6 GPa) torsion deformation, indicating the absence of any phase transformation.

In addition, multiple nanotwins were observed inside the

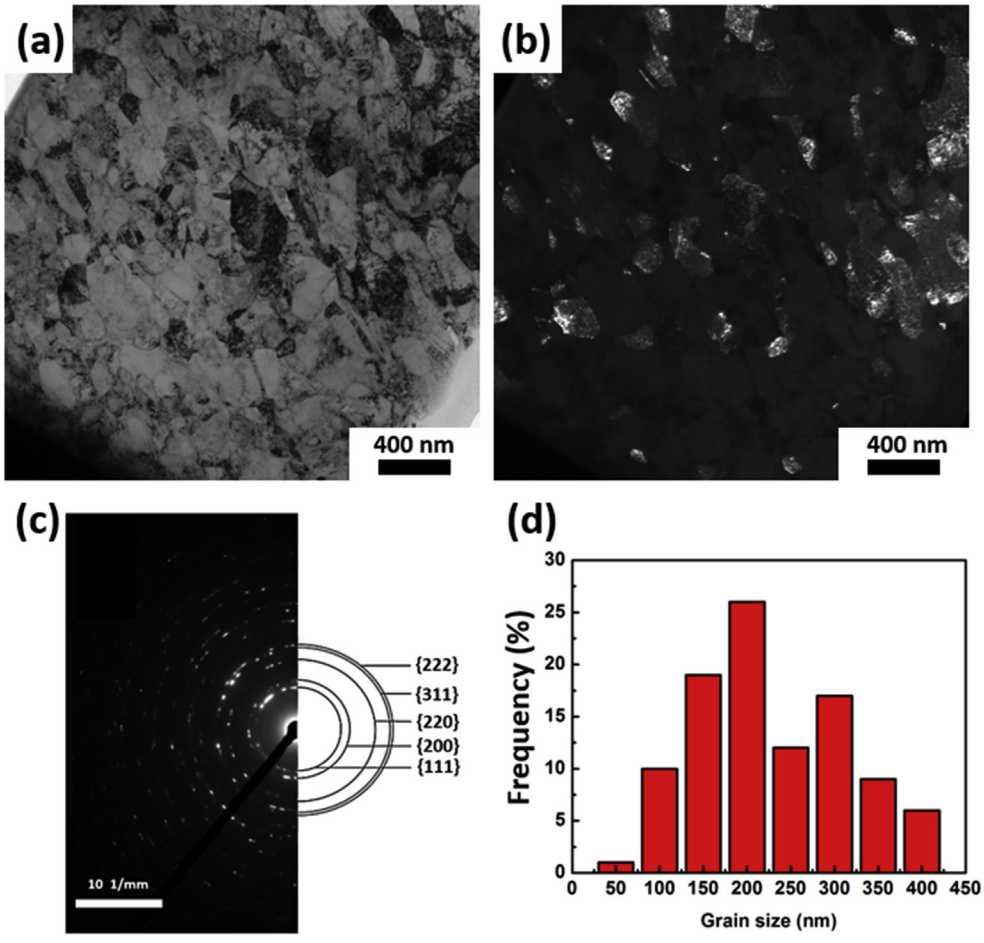

Fig. 5. (a) Bright-field TEM image of the microstructure inside the shear band; (b) corresponding dark-field TEM image of (a); (c) TEM selected area diffraction pattern inside the shear band; (d) grain size distribution inside the shear band corresponding to the TEM image in (a).

recrystallized grains in Fig. 6(a). Meyers and Pak [42] were among the first to identify the ultrafine grained structure in what was, at the time, considered 'transformed' shear bands. This led to the proposal of a rotational recrystallization mechanism [3,42], after observations of ultra-fine grains in AISI 4340 steel [20], stainless steel [21], shock-hardened copper [22], zirconium [23], and titanium [24]. This rotational mechanism explains the formation of equiaxed recrystallized grains inside the adiabatic shear bands, since the deformation time is insufficient for the grain-boundary migration required in conventional recrystallization. The low stacking-fault energy ($\gamma = 21$ mJ/m^2) of the AISI 304 stainless steel (Fe–18%Cr–8%Ni) is on the same order as that of the HEA studied here [21]. The evolution of plastic deformation, coupled with temperature rise, leads to the formation of a dislocated/twinned/transformed microstructure that breaks up the initial grains into small regions. Meyers et al. [43] showed that these local grain-boundary segments, if having dimensions of ~100 nm, can rotate by 30° within the deformation time (estimated to be between 10 and 50 μs) and generate an equiaxed nanostructured structure. Hines and Vecchio [44] and Hines et al. [45] used crystal plasticity theory to predict the evolution of subgrain misorientations during the adiabatic shear localization. By using a bimodal approach, Hines et al. [45] demonstrated that the grains with low angle grain boundaries can rotate, leading to the increase of subgrain misorientation under severe plastic deformation. The elongated grains are proposed to be the first stage of severe shear deformation; they subsequently break up into small ultrafine-grained grains. Fig. 6(b) shows the equiaxed refined grains with arrays of planar dislocations, indicating that they can still be the carriers of plastic deformation at a relatively high temperature inside the shear band. Figs. 6(c) and (d) depict the formation of nanotwins in the recrystallized grains. It is proposed that the formation of nanotwins is promoted by the low stacking-fault energy of this HEA. Interestingly, even negative stacking-fault energies of the fcc CrCoNi and CrFeCoNi alloys have been reported by Zhang et al. [46] and Smith et al. [47]. They attributed this to the thermodynamic metastability of the fcc stacking sequence which is significantly influenced by the local atomic environment in solid solution.

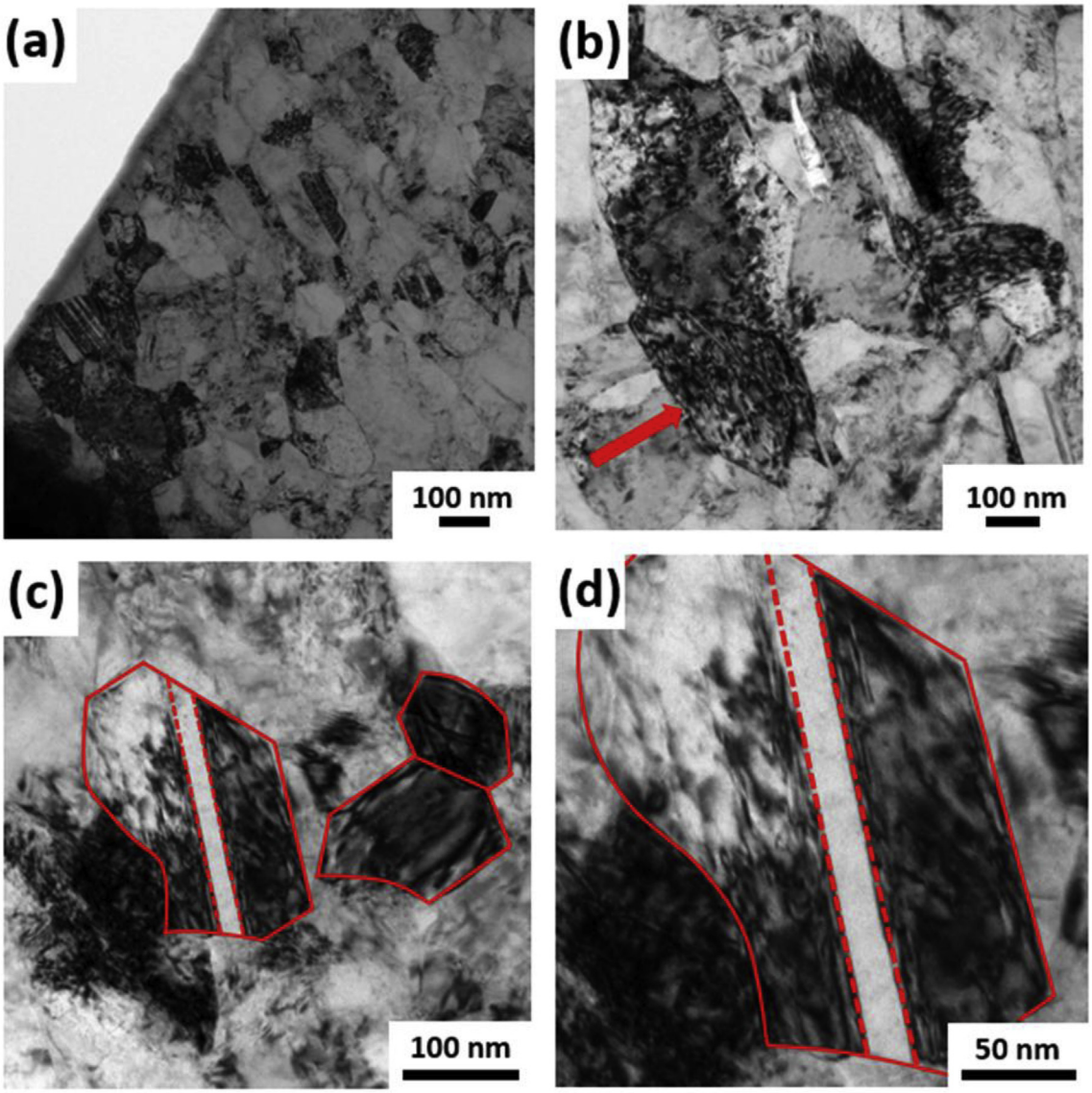

Fig. 6. Bright-field TEM images showing (a) recrystallized grains with dislocations and twins; (b) recrystallized grains with arrays of planar dislocations; (c) recrystallized equiaxed grains with dashed lines showing twin boundaries; (d) nanotwin inside one recrystallized grain.

It is well established that low stacking-fault energy leads to low rates of recovery because the dislocations are sufficiently dissociated so that their climb and cross-slip are difficult [48]. Zhilyaev et al. [49] reported that the stacking-fault energy significantly affected the minimum grain size in severe plastic deformation: a decrease in energy leads to a corresponding decrease in the grain size after processing by HPT under the same experimental condition from copper to bronze to brass. A low stacking-fault energy, and therefore a low rate of recovery, is conducive for attaining an exceptionally small grain size. The CrMnFeCoNi HEA (with stacking-fault energy ~20 mJ/m^2 [17]) attains nanocrystalline grains inside the shear band under severe plastic deformation. The arrays of planar dislocations inside the recrystallized grain is depicted by the red arrow in Fig. 6(b), indicating multiple slip activity.

The twin-boundary energy, γ_{TB}, is proportional to the stacking-fault energy, γ_{SF}, for most metals [50]: $\gamma_{TB} \approx 2\gamma_{SF}$. A high density of recrystallization twins is formed in the CrMnFeCoNi high entropy alloy during dynamic recrystallization inside the shear band. Fig. 6(c) and (d) show nanotwins inside recrystallized grains. The twin boundaries have been marked by the red dashed lines. Similar twin boundaries inside nanostructured grains have also been observed under severe plastic deformation [51]. The “pop-out” mechanism [16,52] does not require concurrent grain-boundary movement for the formation of recrystallization (or annealing) twins and is therefore a possible mechanism, enabled by the lower stacking-fault energy. This provides a method to make nanocrystalline HEAs with twin boundaries and their properties still need to be explored.

4. Concluding remarks

As a summary, the dynamic mechanical behavior of the single phase (fcc) CrMnFeCoNi HEA was examined. This alloy exhibits a high work-hardening rate ~1100 MPa at a true strain of 0.2. The resistance to adiabatic shear localization of this alloy was studied by dynamically-loading hat-shaped specimens. The formation of an adiabatic shear band (with a thickness ~10 μm) requires a very large imposed shear strain of ~7. It is proposed that the combination of the excellent strain-hardening ability and moderate thermal-softening lead to a high resistance of the Cantor alloy to shear localization. A structure consisting of recrystallized ultrafine-grained grains with twins was revealed inside the shear band and is attributed to rotational dynamic recrystallization, a mechanism prevalent in severe plastic deformation.

Acknowledgements

We thank the Department of Energy NNSA/SSAP (DE-NA0002080) for partial support and a UC Research Laboratories Grant (09-LR-06-118456-MEYM). Support of Zezhou Li by China Scholarship Council (201508020004) and of S.M. Alotaibi by Saudi Aramco is gratefully acknowledged. We greatly thank Prof. Olivia Graeve and Arash Yazdani for the help on the XRD experiment. We thank the support by the National Natural Science of China (No. 51771231, 51671217).

References

[1] M.A. Meyers, Dynamic Behavior of Materials, John Wiley & Sons, 1994.
[2] M.A. Meyers, A. Mishra, D.J. Benson, Mechanical properties of nanocrystalline materials, Prog. Mater. Sci. 51 (2006) 427–556.
[3] M.A. Meyers, V.F. Nesterenko, J.C. LaSalvia, Q. Xue, Shear localization in dynamic deformation of materials: microstructural evolution and self-organization, Mater. Sci. Eng., A 317 (2001) 204–225.
[4] Y.S. Li, Y. Zhang, N.R. Tao, K. Lu, Effect of the Zener–Hollomon parameter on the microstructures and mechanical properties of Cu subjected to plastic deformation, Acta Mater. 57 (2009) 761–772.
[5] J.-W. Yeh, S.-K. Chen, S.-J. Lin, J.-Y. Gan, T.-S. Chin, T.-T. Shun, C.-H. Tsau, S.-Y. Chang, Nanostructured high-entropy alloys with multiple principal elements: novel alloy design concepts and outcomes, Adv. Eng. Mater. 6 (2004) 299–303.
[6] B. Cantor, I.T.H. Chang, P. Knight, A.J.B. Vincent, Microstructural development in equiatomic multicomponent alloys, Mater. Sci. Eng., A 375–377 (2004) 213–218.
[7] B. Gludovatz, A. Hohenwarter, D. Catoor, E.H. Chang, E.P. George, R.O. Ritchie, A fracture-resistant high-entropy alloy for cryogenic applications, Science 345 (2014) 1153–1158.
[8] Z. Zhang, M.M. Mao, J. Wang, B. Gludovatz, Z. Zhang, S.X. Mao, E.P. George, Q. Yu, R.O. Ritchie, Nanoscale origins of the damage tolerance of the high-entropy alloy CrMnFeCoNi, Nat. Commun. 6 (2015) 10143.
[9] Y. Zhang, T. Zuo, Z. Tang, M.C. Gao, K.A. Dahmen, P.K. Liaw, Z. Lu, Microstructures and properties of high-entropy alloys, Prog. Mater. Sci. 61 (2014) 1–93.
[10] Z. Li, K.G. Pradeep, Y. Deng, D. Raabe, C.C. Tasan, Metastable high-entropy dual-phase alloys overcome the strength-ductility trade-off, Nature 524 (2016) 227–230.
[11] L.J. Santodonato, Y. Zhang, M. Feygenson, C.M. Parish, M.C. Gao, R.J. Weber, J.C. Neuefeind, Z. Tang, P.K. Liaw, Deviation from high-entropy configurations in the atomic distributions of a multi-principal-element alloy, Nat. Commun. 6 (2015) 5964.
[12] Z. Tang, T. Yuan, C.-W. Tsai, J.-W. Yeh, C.D. Lundin, P.K. Liaw, Fatigue behavior of a wrought $Al_{0.5}$CoCrCuFeNi two-phase high-entropy alloy, Acta Mater. 99 (2015) 247–258.
[13] M.A. Hemphill, T. Yuan, G.Y. Wang, J.W. Yeh, C.W. Tsai, A. Chuang, P.K. Liaw, Fatigue behavior of $Al_{0.5}$CoCrCuFeNi high entropy alloys, Acta Mater. 60 (2012) 5723–5734.
[14] B. Wang, A. Fu, X. Huang, B. Liu, Y. Liu, Z. Li, X. Zan, Mechanical properties and microstructure of the CoCrFeMnNi high-entropy alloy under high strain rate compression, J. Mater. Eng. Perform. 25 (2016) 2985–2992.
[15] Metals Handbook: Metallography and Microstructures, American Society for Metals, Metals Park, OH, 1985 vol. 9.
[16] M.A. Meyers, C. McCowan, The formation of annealing twins: overview and new thoughts, Interf. Mig. Cont. Microst (1984) 99–123.
[17] A.J. Zaddach, C. Niu, C.C. Koch, D.L. Irving, Mechanical properties and stacking fault energies of NiFeCrCoMn high-entropy alloy, J. Mater. 65 (2013) 1780–1789.
[18] H. Zhang, Y.-Z. He, Y. Pan, S. Guo, Thermally stable laser cladded CoCrCuFeNi high-entropy alloy coating with low stacking fault energy, J. of All. and Comp 600 (2014) 210–214.
[19] L.W. Meyer, S. Manwaring, Metallurgical Applications of Shock-wave and High-strain-rate Phenomena, Marcel Dekker, 1986, pp. 657–674.
[20] C.L. Wittman, M.A. Meyers, H.-r. Pak, Observation of an adiabatic shear band in AISI 4340 steel by high-voltage transmission electron microscopy, Metall. Trans. A 21 (1990) 707–716.
[21] M.A. Meyers, Y.B. Xu, Q. Xue, M.T. Pérez-Prado, T.R. McNelley, Microstructural evolution in adiabatic shear localization in stainless steel, Acta Mater. 51 (2003) 1307–1325.
[22] U. Andrade, M.A. Meyers, K.S. Vecchio, A.H. Chokshi, Dynamic recrystallization in high-strain, high-strain-rate plastic deformation of copper, Acta Metall. 42 (1994) 3183–3195.
[23] B.K. Kad, J.-M. Gebert, M.T. Perez-Prado, M.E. Kassner, M.A. Meyers, Ultrafine-grain-sized zirconium by dynamic deformation, Acta Mater. 16 (2006) 4111–4127.
[24] Z. Li, B. Wang, S. Zhao, R.Z. Valiev, K.S. Vecchio, M.A. Meyers, Dynamic deformation and failure of ultrafine-grained titanium, Acta Mater. 125 (2017) 210–218.
[25] G. Laplanche, P. Gadaud, O. Horst, F. Otto, G. Eggeler, E.P. George, Temperature dependencies of the elastic moduli and thermal expansion coefficient of an equiatomic, single-phase CoCrFeMnNi high-entropy alloy, J. of All. Comp 623 (2015) 348–353.
[26] W.-M. Choi, S. Jung, Y.H. Jo, S. Lee, B.-J. Lee, Design of new face-centered cubic high entropy alloys by thermodynamic calculation, Met. Mater. Int 23 (2017) 839–847.
[27] R.F. Recht, Catastrophic thermoplastic shear, J. Appl. Mech. 31 (1964) 186–193.
[28] Z. Li, S. Zhao, H. Diao, P.K. Liaw, M.A. Meyers, High-velocity deformation of $Al_{0.3}$CoCrFeNi high-entropy alloy: remarkable resistance to shear failure, Sci. Rep. 7 (2016) 42742.
[29] F. Otto, A. Dlouhý, Ch Somsen, H. Bei, G. Eggeler, E.P. George, The influences of temperature and microstructure on the tensile properties of a CoCrFeMnNi high-entropy alloy, Acta Mater. 61 (2013) 5743–5755.
[30] M.R. Staker, The relation between adiabatic shear instability strain and material properties, Acta Metall. 29 (1981) 683–689.
[31] R.S. Culver, in: R.W. Rohde, et al. (Eds.), Metallurgical Effects at High Strain Rates, Plenum Press, 1973.
[32] M.A. Meyers, G. Subhash, B.K. Kad, L. Prasad, Evolution of microstructure and shear-band formation in α-hcp titanium, Mech. Mater. 17 (1994) 175–193.
[33] Q. Xue, M.A. Meyers, V.F. Nesterenko, Self-organization of shear bands in titanium and Ti–6Al–4V alloy, Acta Mater. 50 (2002) 575–596.
[34] U.S. Lindholm, G.R. Johnson, Strain-rate Effects in Metals at Large Shear

Strains, Material Behavior under High Stress and Ultrahigh Loading Rates, Springer US, 1983, pp. 61–79.
[35] B. Gludovatz, E.P. George, R.O. Ritchie, Processing, microstructure and mechanical properties of the CrMnFeCoNi high-entropy alloy, J. Mater. 67 (2015) 2262–2270.
[36] G.R. Johnson, J.M. Hoegfeldt, U.S. Lindholm, A. Nagy, Response of various metals to large torsional strains over a large range of strain rates—Part 1: ductile metals, J. Eng. Mater. Technol. 105 (1983) 42–47.
[37] M. Laurent-Brocq, A. Akhatova, L. Perrière, S. Chebini, X. Sauvage, E. Leroy, Y. Champion, Insights into the phase diagram of the CrMnFeCoNi high entropy alloy, Acta Mater. 88 (2015) 355–365.
[38] D. Dudzinski, A. Devillez, A. Moufki, D. Larrouquere, V. Zerrouki, J. Vigneau, A review of developments towards dry and high speed machining of Inconel 718 alloy, Int. J. Mach. Tool Manufact. 4 (2004) 439–456.
[39] D.B. Miracle, O.N. Senkov, A critical review of high entropy alloys and related concepts, Acta Mater. 122 (2017) 448–511.
[40] K.-Y. Tsai, M.-H. Tsai, J.-W. Yeh, Sluggish diffusion in Co–Cr–Fe–Mn–Ni high-entropy alloys, Acta Mater. 61 (2013) 4887–4897.
[41] D.H. Lee, M.Y. Seok, Y. Zhao, I.C. Choi, J. He, Z. Lu, J.Y. Suh, U. Ramamurty, M. Kawasaki, T.G. Langdon, J.I. Jang, Spherical nanoindentation creep behavior of nanocrystalline and coarse-grained CoCrFeMnNi high-entropy alloys, Acta Mater. 109 (2016) 314–322.
[42] M.A. Meyers, H.-r. Pak, Observation of an adiabatic shear band in titanium by high-voltage transmission electron microscopy, Acta Metall. 34 (1986) 2493–2499.
[43] M.A. Meyers, J.C. LaSalvia, V.F. Nesterenko, Y.J. Chen, B.K. Kad, Dynamic recrystallization in high strain rate deformation, Recrystallization and Related Phenomena, Rex'96, in: T.R. McNelley (Ed.), Monterey: the Third International Conference on Recrystallization and Related Phenomena, 1997, pp. 279–286.
[44] J.A. Hines, K.S. Vecchio, Recrystallization kinetics within adiabatic shear bands, Acta Mater. 45 (1997) 635–649.
[45] J.A. Hines, K.S. Vecchio, S. Ahzi, A model for microstructure evolution in adiabatic shear bands, Metall. Mater. Trans. A 29 (1998) 191–203.
[46] Y.H. Zhang, Y. Zhuang, A. Hu, J.J. Kai, C.T. Liu, The origin of negative stacking fault energies and nano-twin formation in face-centered cubic high entropy alloys, Scripta Mater. 130 (2017) 96–99.
[47] T.M. Smith, M.S. Hooshmand, B.D. Esser, F. Otto, D.W. McComb, E.P. George, M. Ghazisaeidi, M.J. Mills, Atomic-scale characterization and modeling of 60° dislocations in a high-entropy alloy, Acta Mater. 110 (2016) 352–363.
[48] F.I. Grace, M.C. Inman, Influence of stacking fault energy on dislocation configurations in shock-deformed metals, Metallography 3 (1970) 89–98.
[49] A.P. Zhilyaev, T.G. Langdon, Using high-pressure torsion for metal processing: fundamentals and applications, Prog. Mater. Sci. 53 (2008) 893–979.
[50] M.A. Meyers, O. Vöhringer, V.A. Lubarda, The onset of twinning in metals: a constitutive description, Acta Mater. 49 (2001) 4025–4039.
[51] B. Schuh, F. Mendez-Martin, B. Völker, E.P. George, H. Clemens, R. Pippan, A. Hohenwarter, Mechanical properties, microstructure and thermal stability of a nanocrystalline CoCrFeMnNi high-entropy alloy after severe plastic deformation, Acta Mater. 96 (2015) 258–268.
[52] M.A. Meyers, L.E. Murr, A model for the formation of annealing twins in F.C.C. metals and alloys, Acta Metall. 26 (1978) 951–962.